

THE OFFICIAL MAGAZINE OF THE OCEANOGRAPHY SOCIETY

# Oceanography

#### CITATION

Nash, J.D., E.L. Shroyer, S.M. Kelly, M.E. Inall, T.F. Duda, M.D. Levine, N.L. Jones, and R.C. Musgrave. 2012. Are any coastal internal tides predictable? *Oceanography* 25(2):80–95, <http://dx.doi.org/10.5670/oceanog.2012.44>.

#### DOI

<http://dx.doi.org/10.5670/oceanog.2012.44>

#### COPYRIGHT

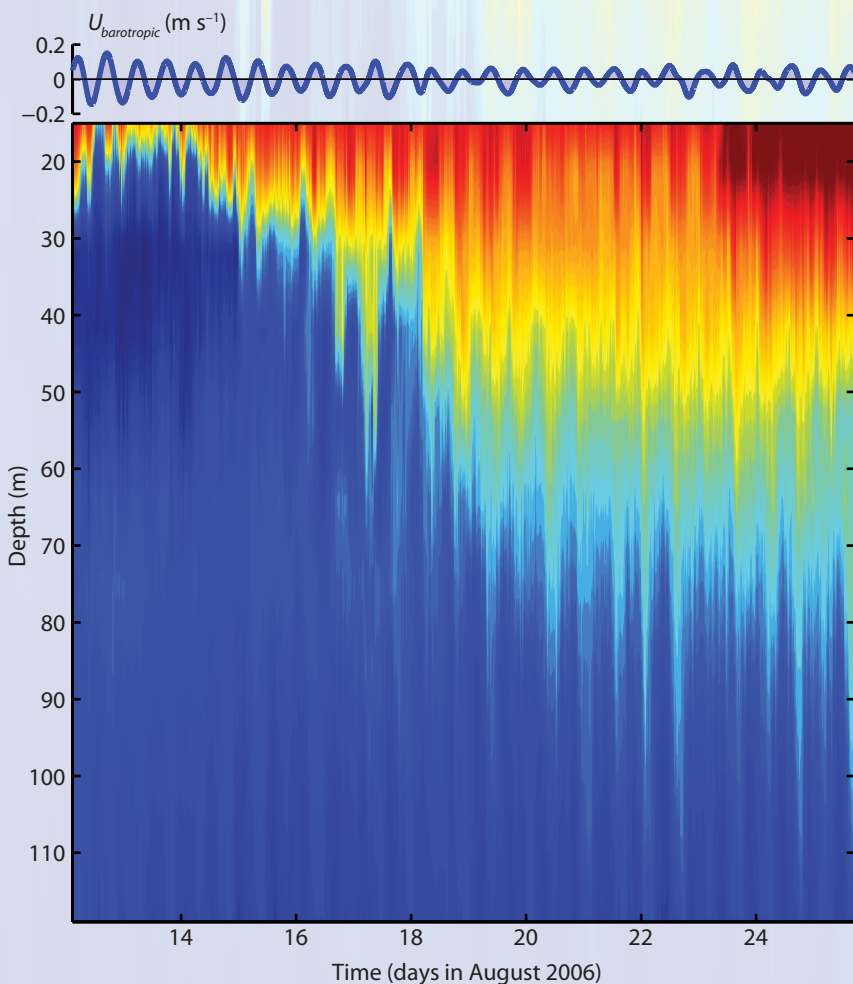
This article has been published in *Oceanography*, Volume 25, Number 2, a quarterly journal of The Oceanography Society. Copyright 2012 by The Oceanography Society. All rights reserved.

#### USAGE

Permission is granted to copy this article for use in teaching and research. Republication, systematic reproduction, or collective redistribution of any portion of this article by photocopy machine, reposting, or other means is permitted only with the approval of The Oceanography Society. Send all correspondence to: [info@tos.org](mailto:info@tos.org) or The Oceanography Society, PO Box 1931, Rockville, MD 20849-1931, USA.

# Are Any Coastal Internal Tides Predictable?

BY JONATHAN D. NASH, EMILY L. SHROYER, SAMUEL M. KELLY,  
 MARK E. INALL, TIMOTHY F. DUDA, MURRAY D. LEVINE,  
 NICOLE L. JONES, AND RUTH C. MUSGRAVE



**ABSTRACT.** Surface tides are the heartbeat of the ocean. Because they are controlled by Earth’s motion relative to other astronomical objects in our solar system, surface tides act like clockwork and generate highly deterministic ebb and flow familiar to all mariners. In contrast, baroclinic motions at tidal frequencies are much more stochastic, owing to complexities in how these internal motions are generated and propagate. Here, we present analysis of current records from continental margins worldwide to illustrate that coastal internal tides are largely unpredictable. This conclusion has numerous implications for coastal processes, as across-shelf exchange and vertical mixing are, in many cases, strongly influenced by the internal wave field.

A two-week record of barotropic velocity (top) and temperature (bottom) from the New Jersey shelf illustrate the complexity of internal tides in a temporally evolving coastal climate. In this case, the internal tide is strongly decoupled from the barotropic forcing; shoaling internal tides from remote locations are believed to influence its variability.

## INTRODUCTION

It may seem odd to use the term “intermittent” when discussing tides. We usually think of tides as being precise oscillations of the ocean that are forced by the gravitational attraction of the Moon and Sun. Indeed, this is the case for surface, or *barotropic*, tides. Barotropic tides can often be described as linear shallow-water gravity waves because their horizontal wavelengths are much greater than the water depth. As the tide moves the sea surface up and down, the horizontal water velocity is nearly uniform with depth.

The *internal tide* is a different type of wave altogether (Wunsch, 1975). Because the ocean is vertically stratified according to density, oscillations on internal interfaces are possible, supporting what are called internal gravity waves. An internal tide is an internal gravity wave that is generated at a tidal frequency by the interaction of the barotropic tide with topography. Hence, astronomical gravitational forces do not directly generate internal tides. Internal tides can be pictured as perturbations in density surfaces that propagate horizontally like sine waves. Unlike the barotropic tide, wave patterns of the internal tide vary with depth because perturbations on each density surface may differ slightly in phase, amplitude, and frequency. Internal tides also differ from the surface tide because their horizontal wave speeds are much slower than those of shallow-water waves. This slower speed results from internal density differences that are much less than the density difference at the air/sea interface, and so the natural oscillations of internal perturbations are much slower than perturbations on the sea surface.

Internal tides represent a significant contribution to the internal motions that occur on many continental shelves (e.g., MacKinnon and Gregg, 2003), and they are often a dominant energy source for turbulent mixing and other transports (e.g., Green et al., 2008; Shroyer et al., 2010a). As a result, they can control the timing of phytoplankton blooms (through nutrient upwelling; e.g., Briscoe, 1984) and drive horizontal transports in the shallow inner shelf (e.g., Pineda, 1999). In addition, they can manifest themselves into large-amplitude internal waves and bores. These internal waves and bores can produce strong surface convergences and/or intense near-bottom currents (Moum et al., 2008) that can be a hazard to maritime operations or stress offshore structures (Osborne et al., 1978; Holloway et al., 2001). Numerous studies (e.g., Boehm et al., 2002; Noble et al., 2009) also implicate these nonlinear internal tides in cross-shore transport to the surfzone, so quantifying their influence has practical importance for locating sewage outfalls. We care about predicting internal tides because their energy can change by an order of magnitude on seasonal and shorter timescales. Such variability may represent a dominant control on the frequency and timing of the internal tide impacts in the coastal environment. For example, if larval recruitment or the occurrence of harmful algal blooms can be tied to the internal tide, could they be predicted?

Understanding regional predictability of internal tides is also relevant to coupled physics-ecosystem model predictions of shelf seas productivity and their capacity to draw down CO<sub>2</sub> from the atmosphere. Shelf seas are understood to be highly productive, sequestering up

to 40% of the global annual export of particulate organic carbon (Thomas et al., 2004). In summertime, this production is largely fueled by vertical nitrate flux into the nutrient-depleted surface waters mediated by the internal tide's energy. Large spring/neap variations in this flux have been reported (Sharples et al., 2007), and it follows that intermittency in the internal tide may significantly influence the distribution of summertime vertical nutrient fluxes in shelf seas.

The internal tide is much less predictable than the barotropic tide for two key reasons (see Box 1: The Bandwidth of Tides). First, the barotropic tide is forced directly at the precise frequencies of astronomical gravitational forces. The ocean basins respond cleanly to this forcing because the amplitude of the response (e.g., sea surface height oscillations) is much larger than other oceanographic variability, even in complex coastal regions. Additionally, the ocean's density stratification has only a minor effect on modulating the barotropic response to astronomic tidal forcing. In contrast, the internal tide is generated indirectly from astronomical forcing through the action of raising the stratified ocean up and down along sloping topography by the barotropic tidal currents. Therefore, the phases, amplitudes, and generation locations of the internal tide change as the ocean's stratification evolves (Gerkema et al., 2004).

Second, the spatial and temporal variability of the oceanic background density and current fields affects the internal tide to a greater extent than the barotropic tide because internal-tide wave speeds are similar in magnitude to other oceanographic variability, for example, near-inertial motions, geostrophic currents,

## BOX 1 | THE BANDWIDTH OF TIDES

The astronomical forcing that generates the barotropic tide can be thought of as a sum of forces, each oscillating at a different precise frequency. However, the ability to resolve the frequency of such an oscillation is determined by the total duration of the oscillation. The longer the oscillation's duration, the more precisely its frequency can be resolved. To illustrate with an example, look at a power spectrum that shows the energy of the signal as a function of frequency. A signal that has been oscillating forever (infinite duration) appears as a *line spectrum* at four exact tidal frequencies (panel a, black arrows). The same sine wave analyzed over a shorter duration, say 90 days (dark gray line), has a spectrum that is no longer a sharp line, but now has energy spread over a finite frequency band of width  $\sim 1/(90 \text{ days})$  (called the *bandwidth*); analyzed over a 15-day period, the spread and bandwidth are even larger (light gray line). The shorter the duration, the wider the bandwidth and the less precisely the frequency can be determined (i.e., more frequencies are attributed to each spectral estimate). This inverse relationship between the duration of the signal and resolving the frequency is a form of the famous Schrödinger uncertainty.

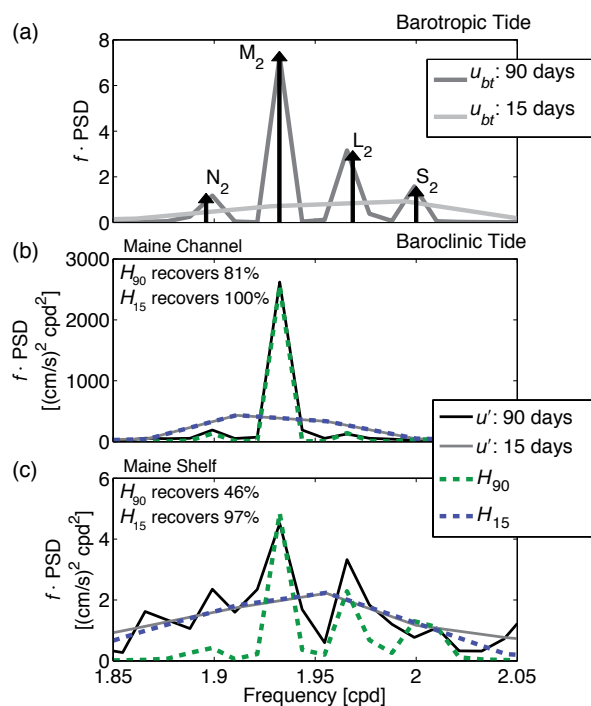
Because the barotropic tide is strongly coupled to astronomical forcing, it is well represented by oscillations at precise frequencies over long durations. The barotropic tidal response is approximately the sum of discrete spectral lines, as schematically illustrated by the black arrows in panel a. The internal tide is much less regular. Although the barotropic tide, which forces the internal tide, is at fairly precise frequencies, ocean stratification varies in time, affecting the internal tidal response. Furthermore, as the internal tide propagates through the ocean, background currents and stratification refract the waves. Thus, the internal tide often appears as oscillations with slowly varying frequency and amplitude. Hence, the spectral peaks are broader and have greater bandwidth than barotropic tides. Another but equivalent way to think of the internal tide is that the signal has been smeared over a greater frequency bandwidth compared with the corresponding precise frequency of the barotropic tide.

The importance of bandwidth is illustrated using example spectra of baroclinic velocity from the Maine Channel and shelf, as shown in panels b and c. Within the channel, the baroclinic  $u'$  for a 90-day duration spectrum is dominated by a single tidal frequency, with small contributions from two neighboring tidal peaks (panel b, black line). The portion of  $u'$  that comes from the tidal frequencies only is  $H_{90}$  (shown by the dashed green line) and represents 81% of the variance of  $u'$ . If the same calculation is performed with 15-day duration spectra ( $u'$  as a gray line, and  $H_{15}$  as a dashed blue line), the three peaks are smeared into the broad semidiurnal band, and there is no ability to differentiate between exact constituent frequencies due to the shortness of the time series. As a result, nearly 100% of the variance of  $u'$  is captured by the discrete tidal

frequencies represented by  $H_{15}$ .

The spectrum from the shelf (panel c) strongly contrasts that from the channel. The raw spectrum (black) is not dominated by a discrete peak, but instead has contributions at many nearby "semidiurnal" frequencies. As a result, only 46% of the variance of  $u'$  can be attributed to the four tidal frequencies represented by  $H_{90}$  (panel c). In contrast, if the data are considered in 15-day periods, the bandwidth is broadened, and all of the variance is distributed into a few frequencies. As in the previous example, the harmonic representation of data using 15 day fits ( $H_{15}$ ) smears all of the variance into a few frequencies, and its spectrum looks similar to that of the raw data over a 15-day duration. As a result, 97% of the variance is explained by  $H_{15}$ .

What does this tell us about predictability? The precise frequencies of the barotropic tide imply accurate predictability. Hence, tide tables based on time series of long duration are quite good. The internal tide would be similarly predictable if there were no frequency smearing by the background current and stratification fields. However, because the background fields are not predictable, the amount of frequency smearing is not predictable either. In this paper, we use the skill of a harmonic fit as a measure of "predictability" in the internal tide. However, this measure only holds for the long time periods. For shorter records, a large bandwidth spread ensures that a large amount of variance will be recovered regardless of how accurately the internal tide can truly be "predicted" from, say, a regional modeling effort. This highlights why the change in  $SS_T$  as a function of  $T$  (e.g., Figure 4) is really what describes the predictability.



and mesoscale eddies. As a result, variation at the mesoscale and submesoscale (i.e., eddies and other ocean variability that produce slowly varying fluctuations in velocity and density over 10–500 km scales) alters an internal tide's propagation speed, causing internal tides to horizontally refract as they radiate from their generation sites (Rainville and Pinkel, 2006). Temporal variation of this background structure also results in Doppler shifting, which alters the arrival times of the internal ebb and flow. Spectrally, this variation in arrival time smears the internal tide over a wider range of observed frequencies, which extend beyond the pure astronomical frequencies that force the barotropic tide (Dushaw et al., 2011). Nonlinear processes, due to interaction of the internal tide with the background fields or topography, can also alter the frequency content of the internal tide. The character of the observed internal tide thus depends on a hierarchy of complex processes, making prediction difficult.

Compared to the open ocean, prediction of the internal tide in coastal regions is perhaps even more challenging due to the above considerations coupled with the large degree of variability found in coastal morphology (e.g., canyons, shoals, and bays), stratification (such as that associated with freshwater runoff or upwelling/downwelling), and circulation (e.g., wind-driven currents and shelf break current systems). A further complication is that the internal tide along the continental margins is influenced by an open-ocean “internal swell” (Alford, 2001, 2003), which may be energetic, temporally intermittent, and generated thousands of kilometers away (Alford and Zhao, 2007). The shoaling of remotely generated internal tides can dominate tidal energetics on continental

slopes, as has been demonstrated offshore of Virginia (Nash et al., 2004) and Oregon (Martini et al., 2011), and can feed into the onshelf internal tide (Nash et al., in press). Not only can this remotely shoaling component interfere directly with the locally generated internal tide to create complex constructive and destructive interference patterns (as noted by Rainville et al., 2010, in the open ocean), it can also constructively or destructively interfere with local surface tides, temporarily enhancing or suppressing local internal-tide generation and adding to the intermittency of the resultant wavefield (Kelly and Nash, 2010). An unfortunate result of these interactions is that internal tides along the continental margins are inexorably coupled to the details of the “internal swell” and, hence, the dynamics of the remote mesoscale.

Nevertheless, in regions where generation is highly localized (e.g., marginal seas with connections to the open ocean via narrow strait systems) and/or where tidal forcing is sufficiently strong compared to other external forcing, internal tides can appear regularly and accurate prediction may be possible. Indeed, observations that demonstrate a highly stationary internal tide tend to be located in semi-enclosed basins and marginal seas, such as Massachusetts Bay (Scotti

et al., 2008), the Bay of Biscay (Pingree and New, 1991; Gerkema et al., 2004), and the South China Sea (Ramp et al., 2010; Li and Farmer, 2011). Conversely, several studies over open continental shelves have noted that the internal tide may exhibit significant low-frequency variability that does not follow the local barotropic spring/neap cycle (Inall et al., 2000; Sherwin et al., 2002; MacKinnon and Gregg, 2003; Lerczak et al., 2003; Savidge et al., 2007; Osborne et al., 2011), suggesting that shoaling internal tides may complicate local dynamics. Open-ocean sites that are largely predictable from surface forcing and stratification tend to be located in regions of strong generation, such as the Hawaiian Ridge (Colosi and Munk, 2006; Lee et al., 2006; Carter et al., 2008; Zilberman et al., 2011), which produces internal tides that dwarf the “internal swell.”

The purpose of this article is to try to understand how intermittency varies on continental margins around the globe.

## METHODOLOGY

A broadband internal tide can be decomposed into two components: (1) a largely predictable component that can be described by a series of tidal frequency sinusoids whose amplitudes and phases vary on timescales much longer than the lowest tidal frequency constituent,

---

**Jonathan D. Nash** ([nash@coas.oregonstate.edu](mailto:nash@coas.oregonstate.edu)) is Associate Professor, College of Earth, Ocean and Atmospheric Sciences, Oregon State University, Corvallis, OR, USA.

**Emily L. Shroyer** is Assistant Professor, College of Earth, Ocean and Atmospheric Sciences, Oregon State University, Corvallis, OR, USA. **Samuel M. Kelly** is Research Fellow, University of Western Australia, Perth, Australia. **Mark E. Inall** is Professor, Scottish Marine Institute, Oban, Scotland. **Timothy F. Duda** is Senior Scientist, Woods Hole Oceanographic Institution, Woods Hole, MA, USA. **Murray D. Levine** is Professor, College of Earth, Ocean and Atmospheric Sciences, Oregon State University, Corvallis, OR, USA. **Nicole L. Jones** is Assistant Professor, University of Western Australia, Perth, Australia. **Ruth C. Musgrave** is PhD Candidate, Scripps Institution of Oceanography, University of California San Diego, La Jolla, CA, USA.

and (2) a largely unpredictable component associated with intermittent pulses of tidal-band energy that arrive with differing phases and amplitudes over much shorter timescales. We will use the terms coherent and incoherent to distinguish between these two internal tide contributions. Note that our use of the word “coherent” does not require that the internal tide be directly related to astronomical forcing, but instead that motions at a fixed location retain a constant phase and amplitude relationship over a given time span.

In this paper, we define the “tidal band” as having broad frequency content that spans 6–30 h periods. Our goal is to assess the timescales over which internal-tide variance retains phase and amplitude coherence, and to determine what fraction of the total broadband signal is explained by a sum of harmonic constituents. To do this evaluation, we perform the following computations. We band-pass filter velocity records to retain 6–30 h variance, and we subtract the depth-mean ( $u_{bt}$ ) to obtain the tidal-band baroclinic velocity ( $u'$ ). We use harmonic analysis to isolate the coherent part of  $u'$ , which is defined as the sum of a series of tidal frequency sinusoids with amplitudes and phases obtained by least squares fitting to the data (i.e., the “harmonic fit”). We compute harmonic fits over a variety of time durations that spanned from 3 to 180 days. Time windows are shifted by 12.5%, and averaged overlapping segments to recreate “running” harmonic fits to  $u'$ . This averaging procedure imposes a degree of phase and amplitude coherence that falls somewhere between periods of  $T$  and  $2T$ . Each depth was treated independently. We define  $H_T$  as the baroclinic time series regenerated from a composite of harmonic analyses of period  $T$  days. Box 1 further discusses decomposition of

a signal into Fourier components.

Here, we define the predictive capability of a harmonic fit using the Skill Score ( $SS_T$ ; Murphy, 1988),

$$SS_T = 100\% \times \left[ 1 - \frac{\langle (u' - H_T(u'))^2 \rangle}{\langle u'^2 \rangle} \right],$$

where  $T$  represents the period (in days) over which the harmonic analysis is performed and the angled brackets indicate averaging over depth and  $T$ . When  $SS_T = 100\%$ , the harmonic fit captures all of the observed baroclinic variance, and when  $SS_T = 0\%$  it captures none of the variance. Note that  $SS_T$  can be negative if the harmonic prediction is anticorrelated with the data over the particular time window.

Throughout this paper, we also use root-mean-square (rms) velocities to characterize the time variability of signals. For barotropic velocities, rms is computed within running 30 h windows (i.e.,  $(\overline{u_{bt}^2})^{1/2}$ ). For baroclinic velocities,  $(\overline{(\dots)^2})^{1/2}$  is computed, where the double overbar represents averaging over the water column and 30 h duration, and (...) represents either  $u'$  (for broadband rms) or  $H_T$  for the rms of a harmonic fit of duration  $T$ . For  $H_{15}$  and  $H_{30}$ , we fit to the following tidal constituents:  $M_2$ ,  $S_2$ ,  $N_2$ ,  $K_1$ ,  $O_1$ ,  $J_1$ .  $H_{90}$  additionally includes  $K_2$  and  $L_2$ , and  $H_{180}$  includes these constituents plus  $P_1$ .

We applied the above methodologies to data from 16 stations located around the world that have almost full-depth velocity coverage (required to separate barotropic and baroclinic motions). Many of the US coastal records were gathered from the archives of the National Data Buoy Center; contributors of other records are listed in the acknowledgements. We extrapolated data to the surface and bottom using

the nearest velocity measurements and assumed constant velocity. Times when missing data spanned more than 33% of the water column were omitted from the analysis. Temporal gaps shorter than three hours were linearly interpolated, and gaps longer than three hours remain in the data records. Data were averaged into one-hour bins before the processing described above was performed.

We note that the chosen 6–30 h pass band contains both near-inertial and tidal band variability (semidiurnal and diurnal). To test whether this broad definition of the internal tide affects our conclusions, we performed a parallel set of analyses in which the pass band was reduced to 9–15 h periods, thereby isolating the semidiurnal tidal band. We found that  $SS_T$  increased by 3–10% depending on site; however, the general tendency for a particular site to be “predictable” versus “unpredictable” did not change. Because these differences are relatively small, we have chosen to present data that include the broad 6–30 h pass band, which includes semidiurnal, diurnal, and near-inertial variability.

## THE INTERNAL TIDE IN THE COASTAL OCEAN—AN EXAMPLE

As an example of what might be considered a “typical” coastal-ocean internal tide, we examine a two-year-long record of  $u$  from the Gulf of Maine (Figure 1). For this time series, we consider harmonic analyses based on durations of 15 and 90 days ( $H_{15}$  and  $H_{90}$ ) and compare them to the tidal-band time series  $u'$ .

From time series spanning a two-year period (Figure 1a), there is evidence of strong seasonal modulation of the internal tide, presumably resulting from increased stratification in the gulf during the summer months, which supports

stronger internal tides (see Box 2: The Timor Sea as an illustration of stratification effects). The internal tide's seasonal cycle is quantified in the upper panel, which indicates that  $\text{rms}(u')$  and  $\text{rms}(H_{90})$  are up to twice as strong (four times the energy) in the summer months, depending on whether the phase-locked (black) or broadband (gray) signals are considered. Similar seasonal modulation of the internal tide has been noted in other coastal ocean settings, such in the Clyde Sea (West Scotland Shelf; Cottier et al., 2004) and the Australian North West Shelf (Hollaway, 1988). Interestingly, there is also a seasonal

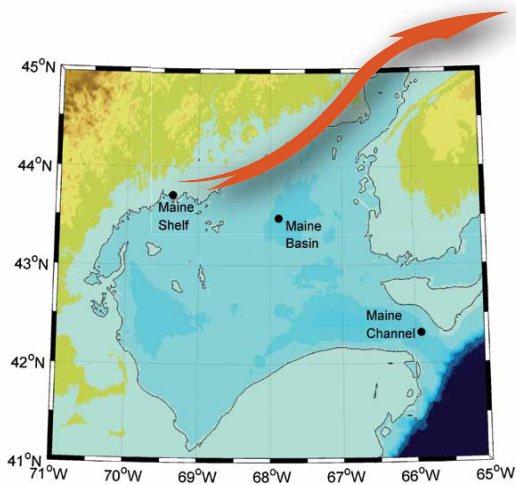
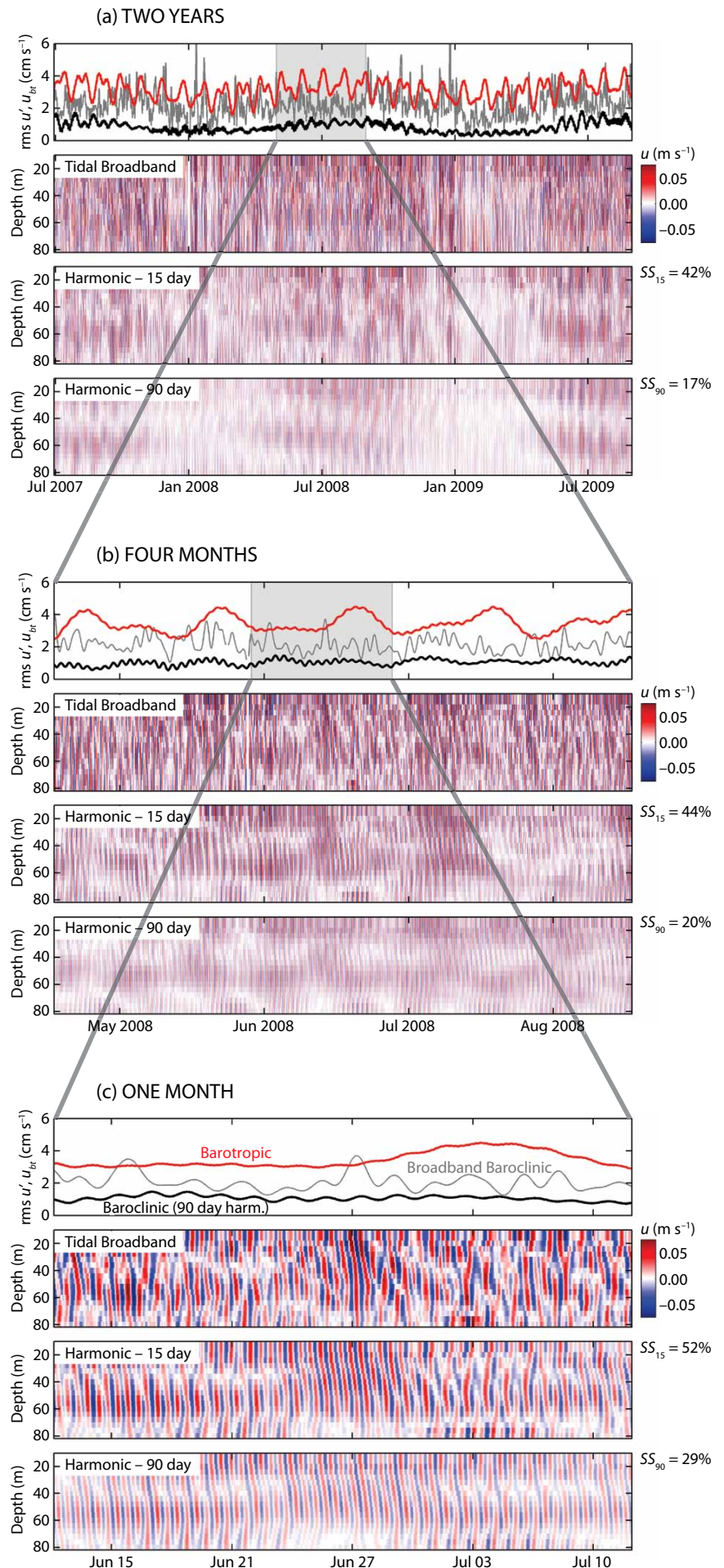


Figure 1. Time series of zonal velocity from the 100 m deep Maine Shelf illustrate variability typical of coastal internal tides. Shown is the same multiyear dataset, zoomed to (a) two years, (b) four months, and (c) one month to highlight the different timescales of coherent signals. The full baroclinic tidal band ( $u'$ ; upper middle panels) is considerably intermittent on annual through several-day timescales. As a result, 15-day harmonic analyses ( $H_{15}$ ; lower middle panels) capture approximately 50% of the tidal variance. Harmonic analyses performed over 90-day periods ( $H_{90}$ ; lower panels) capture only 20–30% of the variance. The one-month record (c) provides a glimpse as to why the vertical structure is patchy and its patterns change almost daily. This type of complex structure can only be partially reproduced by harmonic analyses that capture the fraction of the signal that maintains phase and amplitude coherence over the duration of the analysis period (15 or 90 days in these examples). Line plots above each record show the rms  $u_{bt}$  (red),  $u'$  (gray), and  $H_{90}$  (black).



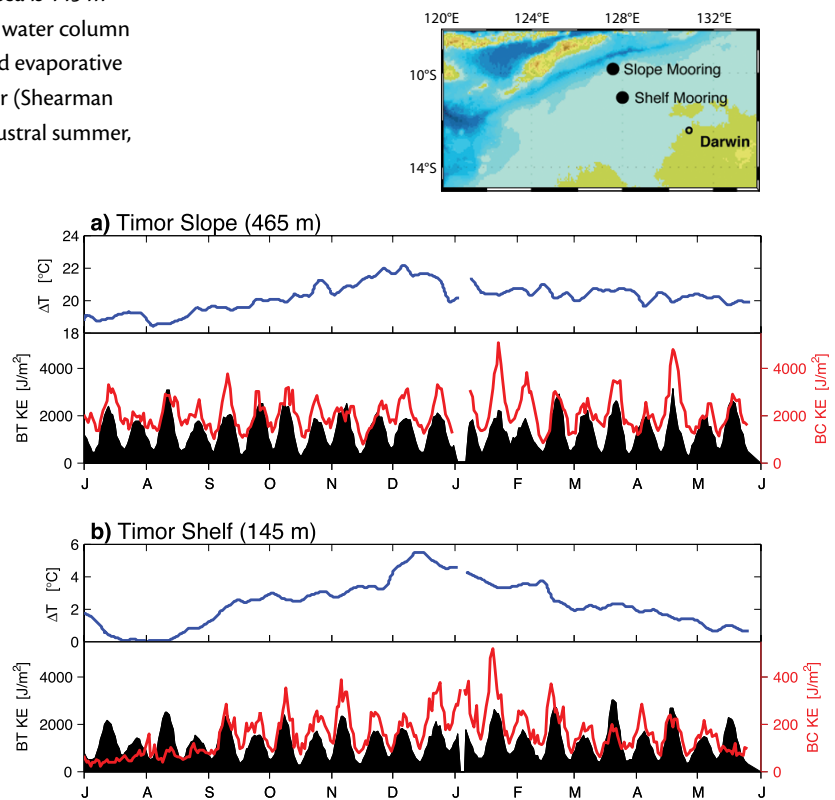
## BOX 2 | THE TIMOR SEA

Some of the largest tides in the world occur on the North West Australian Shelf (NWS) where they dominate local current variability and generate large internal tides. Accurate internal-tide prediction in this region is necessary in order to understand coastal biophysical interactions and to safely extract hydrocarbons from beneath the seafloor. The Timor Sea is located at the northern end of the NWS. As the Timor Sea is a semi-enclosed basin, most internal tides are generated within the sea and should, in theory, be predictable from regional numerical models. However, temporally and spatially variable stratification still produces complicated internal-tide dynamics.

Two moorings illustrate relationships between density stratification, which is inferred from top-to-bottom temperature differences ( $\Delta T$ ), and internal-tide kinetic energy from July 2010 to June 2011. Over the continental slope, where the sea is 465 m deep, the water column is permanently stratified and maintains  $\Delta T \approx 20^\circ\text{C}$  throughout the year. Over the continental shelf, where the sea is 145 m deep, intense shortwave radiation warms the upper water column during the austral summer to produce  $\Delta T \approx 3^\circ\text{C}$ , and evaporative cooling mixes the water column in the austral winter (Shearman and Brink, 2010) to produce  $\Delta T \approx 0^\circ\text{C}$ . During the austral summer, when both slope and shelf waters are stratified, internal tides are observed at both moorings. However, internal tides over the slope are an order of magnitude more energetic than those on the shelf. This difference is attributed, in part, to weaker temperature stratification over the shelf, which inhibits local internal-tide generation (e.g., Baines, 1982). During the austral winter, when stratification weakens slightly over the slope and significantly over the shelf, internal tides at both locations also weaken. However, internal tides over the slope remain energetic because they depend primarily on the deep permanent thermocline (e.g., Gerkema et al., 2004), while internal tides over the shelf weaken when seasonal stratification is completely eroded.

Although internal-tide kinetic energy in the Timor Sea depends on seasonal stratification, it is not linearly or even monotonically related to stratification on shorter timescales. This is in part because the depth structure of stratification influences internal-tide generation and propagation (e.g., Gerkema et al., 2004) through nonlinear processes. For instance, internal tides that are generated during the austral winter on the continental

slope cannot propagate onto the well-mixed shelf and are therefore trapped within the 3,000 m deep Timor Trough. Such trapping may nonlinearly increase or decrease interactions (i.e., resonance) between the internal tides that are generated along the opposite flanks of the trough. As another example, the evolution of stratification on the shelf can influence the efficiency of internal-tide generation at isolated topographic bumps, ravines, and seamounts by altering the locations of slopes that are parallel to semidiurnal internal-wave characteristics (i.e., near critical). Therefore, the locations of internal-tide generation on the shelf evolve with the depth structure of stratification, affecting the strength and directionality of internal tides. Moreover, the evolving mixed-layer depth also influences where tidally forced nonlinear waves are generated and whether they propagate as surges, boluses, or waves of depression/elevation (e.g., Lim et al., 2008).



On the continental slope (a), top-to-bottom temperature stratification (blue) is permanently  $\Delta T \approx 20^\circ\text{C}$  with little seasonal variation. As a result, internal-tide kinetic energy (red, band-averaged over three days) is generated locally by surface tide flow over steep topography and follows the spring/nearest cycle of the surface-tide kinetic energy (black). On the continental shelf (b), temperature stratification (blue, note the different scale) does not exist during winter but is  $\Delta T \approx 3^\circ\text{C}$  during the rest of the year. As a result, internal-tide kinetic energy (red, note the smaller scale) is seasonal and much less energetic than on the slope, despite similar surface-tide kinetic energy (black).



modulation of the barotropic tide in addition to the spring-neap cycle, which dominates the variability in  $\text{rms}(u_{bt})$ .

Examining only the summer of 2008 (Figure 1b),  $u'$  exhibits phase-coherent spring-neap modulation that is captured by the harmonic fits, albeit weaker than that within the barotropic tide (compare red and black lines in the upper panel). At the same time,  $H_{90}$ ,  $H_{15}$ , and tidal-band  $u'$  records exhibit considerable differences, which indicate that variability occurs on multiple timescales. For example, periods of strong near-bottom internal motions, which are found in  $u'$  and  $H_{15}$  during the latter part of May and June 2008, are not captured in  $H_{90}$ . Additionally, neither  $H_{15}$  nor  $H_{90}$  capture the appropriate amplitude of  $u'$  in the early part of August 2008.

Zooming in further to a one-month period (June 12 to July 12; Figure 1c) reveals the complexity of the internal tide, and exemplifies the differing character of  $H_{90}$ ,  $H_{15}$ , and tidal-band records. While the general character of the variability is somewhat captured by  $H_{90}$  and  $H_{15}$ ,  $u'$  is truly broadband—it is characterized by two-to-four-day pulses of semidiurnal and diurnal oscillations, which are modulated on spring/neap and other timescales. This is evident in  $\text{rms}(u')$  that increases by a factor of two during one- to two-day periods (gray curve in upper panel) and that cannot be captured using multiday or multimonh harmonic representations.

The unpredictable pulse-like nature of tidal variability in the Gulf of Maine projects broadly in frequency space so that only a fraction of tidal-band variance is captured by harmonic analyses. The Skill Score, which quantifies the stationarity within the tidal band, indicates that only approximately 50% of  $u'$  is predictable from short-period harmonic fits

( $SS_{15} \sim 42\text{--}52\%$ ), and even less is predictable from longer-term fits ( $SS_{90} \sim 25\%$ ). As will be shown later,  $SS_{15}$  and  $SS_{90}$  vary considerably from region to region, and even among locations in close proximity.

### CONTRASTING THE CHARACTER OF INTERNAL TIDES AT FOUR CONTINENTAL SITES

A closer examination of short time records from locations around the world illustrates the spatial and temporal variability in the internal tide. Inset panels in Figure 2 show tidal currents over three-day time spans at four different locations: the Oregon coast, the Gulf of Maine (NDBC 44024), the Timor Sea, and the Malin Shelf (moving counter-clockwise from the upper-left inset). For each station, we selected three time spans, each with similar barotropic forcing. Comparison of the corresponding tidal-band baroclinic velocity  $u'$  to harmonic fits over 15 and 180 days ( $H_{15}$  and  $H_{180}$ ) demonstrates differences among the locations and the potential (or lack thereof) for predictability.

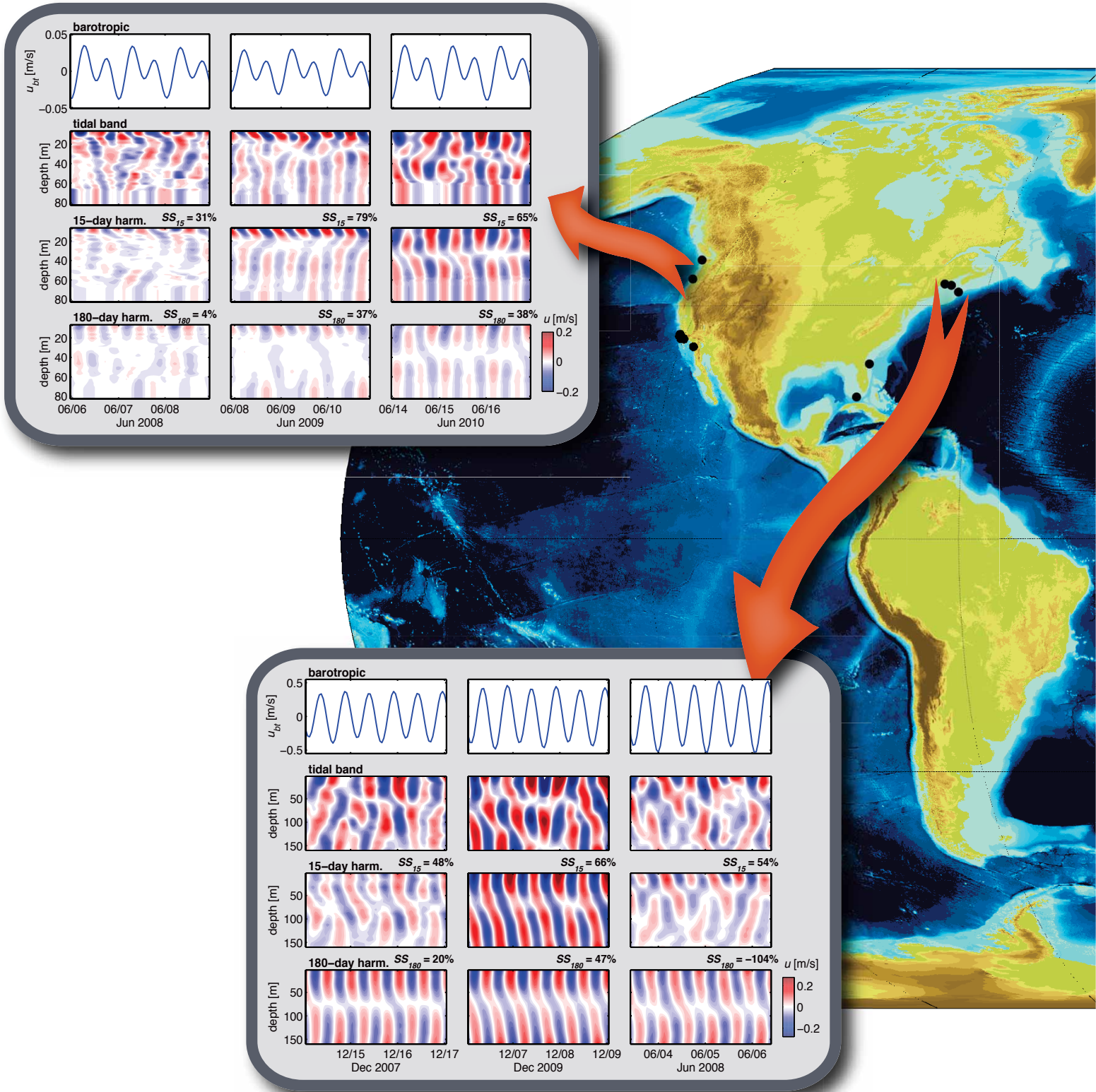
The internal tide over the Oregon Shelf exhibits the highly variable energy levels typical of US West Coast shelves (5–10  $\text{cm s}^{-1}$  rms). Remotely shoaling tides are thought to play a large role in setting the internal tide on this coast (Martini et al., 2011), and a dynamic wind-driven current system can further complicate local internal-tide generation and propagation (Osborne et al., 2011). The three-day time series shown in the upper left inset illustrates these complications during three different summers.  $H_{180}$  captures little of the variance in  $u'$  ( $SS_{180} \sim 4\text{--}38\%$ ), while  $H_{15}$ , which allows for modulation of phase and amplitude on several-week timescales, has relatively high skill ( $SS_{180} \geq 65\%$ ) in June 2009 and

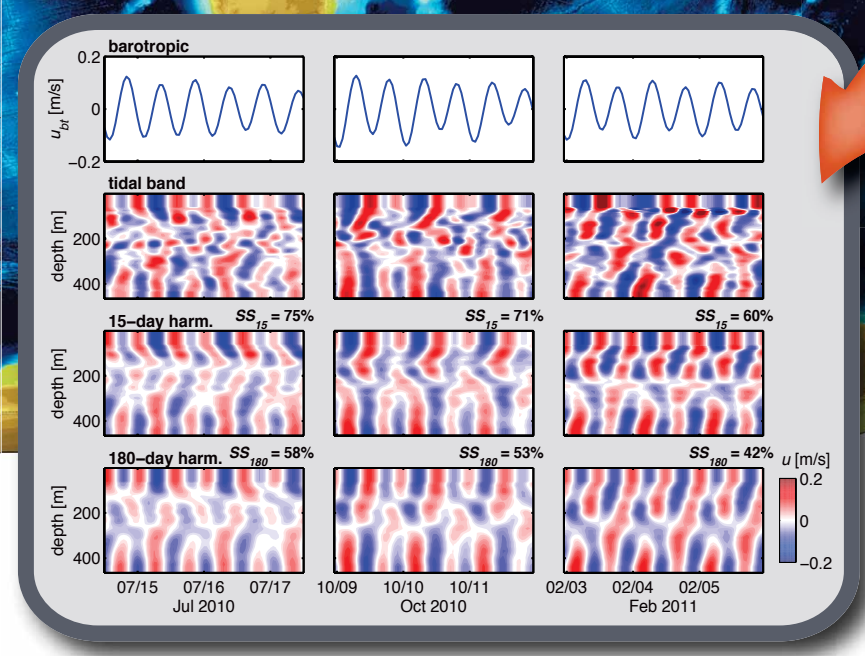
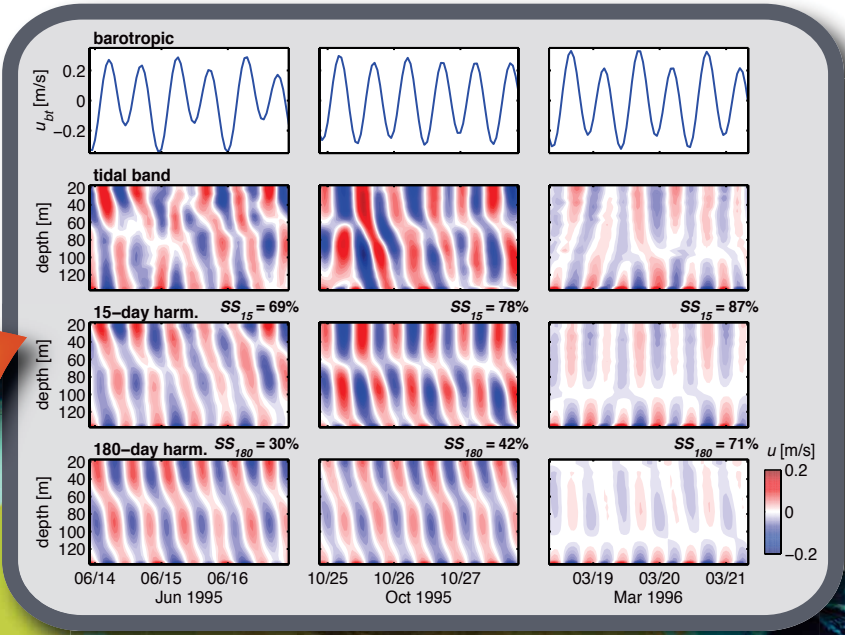
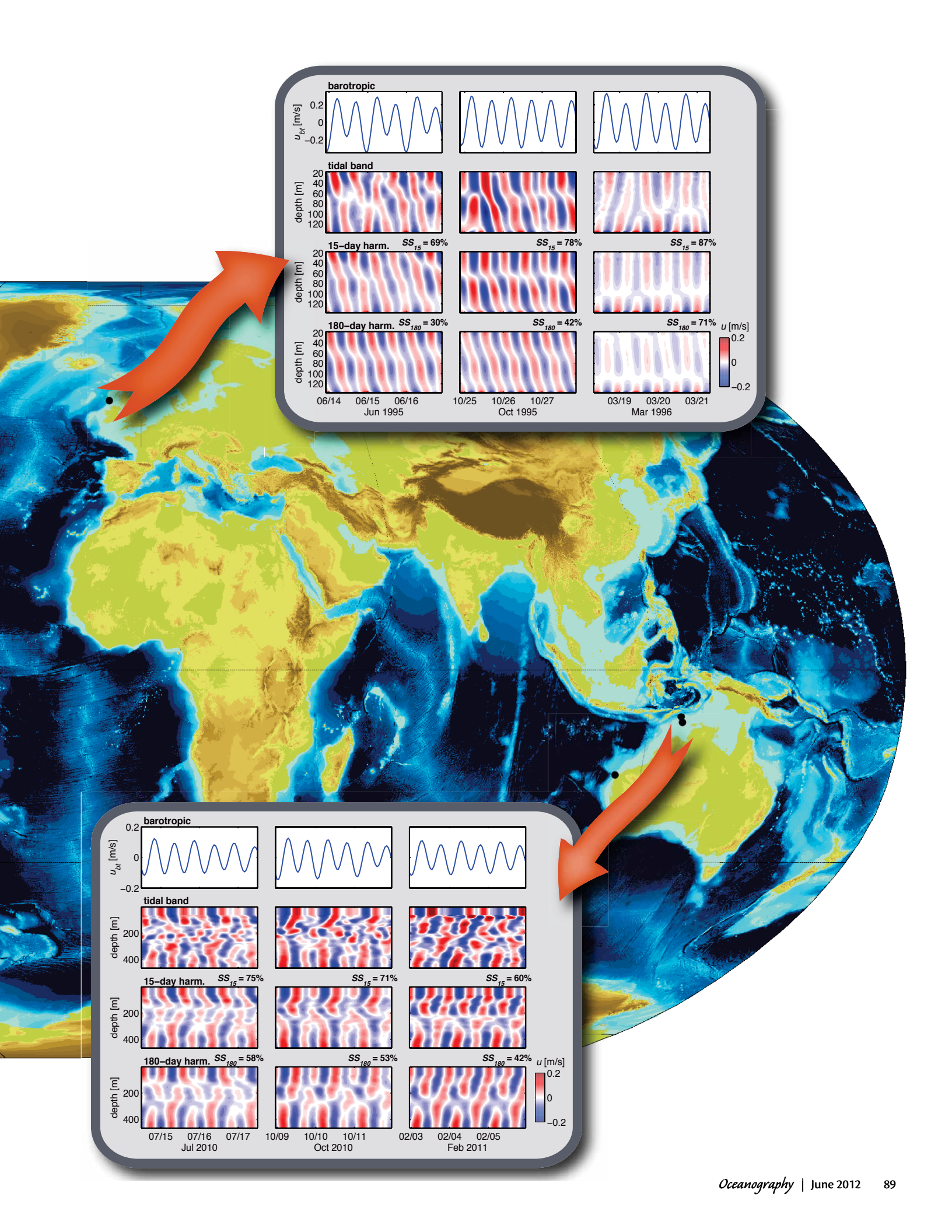
2010. However, the general lack of agreement in June 2008 ( $SS_{15} = 31\%$ ) illustrates that the internal tide is sometimes non-stationary even over short timescales.

The Gulf of Maine exhibits some of the largest barotropic tides in the world (Garrett, 1972), with the innermost region of the resonant area, the Bay of Fundy, being renowned for extreme displacements. Compared to the open and narrow Oregon Shelf, the Gulf of Maine is somewhat sheltered. Accordingly, we might anticipate that local barotropic forcing plays a strong role in determining the internal tide in this location. However, even though the comparatively broad shelf may isolate shelf motions from slope dynamics, it also allows for larger distances over which a shoaling internal tide may be altered by background conditions. While strong seasonality within the Gulf of Maine affects the character of the internal tide, comparison of records for December 2007 and December 2009, which show considerable differences, indicate that seasonality is not the sole factor influencing the internal response. The skill of  $H_{180}$  varies considerably, being very low in December 2007 ( $SS_{180} = 20\%$ ) to reasonable in December 2009 ( $SS_{180} = 47\%$ ) to extremely poor in the case of the June 2008 record ( $SS_{180} = -104\%$ ). In all cases,  $H_{15}$  shows marked improvement, although, as with the Oregon record, its performance is not consistent.

Surface tide amplitudes are large on the Australian North West Shelf and internal tides are ubiquitous features of this region (e.g., Van Gastel et al., 2009; Rayson et al., 2011). In contrast to either of the above cases, a record located on the continental slope of the Timor Sea indicates strong predictability. Regardless of the time of year, a large percentage of the variance in  $u'$  is explained by

Figure 2. World topography with mooring locations indicated by black dots. Insets show barotropic velocity (top panels), baroclinic velocity (second panels), 15-day harmonic fits (third panels), and 180-day harmonic fits (bottom panels) to the baroclinic velocity fields for select mooring locations. Each set of panels shows three-day time periods starting at three different times within the full records. Moving counterclockwise from upper left, those off the coast of Oregon show periods from summer months in three different years (2007, 2009, and 2010), those from the Gulf of Maine show two winter sections (2007 and 2009) and one summer section (2008), and those from the Timor Sea as well as those off the UK show three records, each from a different season.





$H_{15}$  ( $SS_{15} \approx 70\%$ ) and  $H_{180}$  ( $SS_{180} \approx 50\%$ ). High predictability over 180 days is partially attributable to the reduced seasonality in water-column conditions at this site. It is also attributable to the close proximity of this site to regions of intense internal-tide generation. However, a large degree of spatial variability in “predictiveness” is observed in this region (see Box 2).

In common with the ocean margin adjacent to the North West Australian Shelf, barotropic tidal displacements are large along the margin of the Northeast Atlantic, exceeding a meter in most areas. Strong barotropic tides coupled with the broad shelves that are characteristic of this region (i.e., from 200 km wide in the Celtic Sea to  $\sim 50$  km wide around Ireland and with depths typically ranging between 100 and 150 m) result in strong barotropic tidal flow across bathymetric contours and generation of energetic internal tides (Pingree et al., 1986; Sherwin, 1988). The internal tide exhibits significant regional variability over the Northwest European Shelf with the on-shelf energy fluxes ranging from about  $1,000 \text{ W m}^{-1}$  in the Celtic Sea (Inall et al., 2011) to about  $100 \text{ W m}^{-1}$  on the Malin Shelf (Sherwin, 1988). The record shown in Figure 2 is from the Malin Shelf, where  $SS_{15} \approx 80\%$  is among the highest of the shallow shelf records. Unlike the Timor slope, seasonality on the Malin Shelf, which in the late fall results in a complete breakdown of thermal stratification, produces strong changes in the internal tide character between June/October and March. Despite the strong seasonal change,  $H_{180}$  explains a similar fraction of variance on average as that on the Timor slope. The high predictive skill at this location is likely associated with the relative stability of subtidal cross-isobath flow. The

region is predominantly a weakly downwelling system, with a strong and stable northward slope current flowing along contours of  $f/h$  at  $\sim 20 \text{ cm s}^{-1}$  offshore of the shelf break (Souza et al., 2001). The stability of this flow contrasts with that over the Oregon Shelf, where a strong wind-driven response can produce significant variability on synoptic (one-week) timescales (Osborne et al., 2011).

### GLOBAL PATTERNS OF RMS VELOCITY AND ITS PREDICTABILITY

To characterize regional variations in the energy and predictability of internal tides, we contrast rms  $u_{bt}$ ,  $u'$ , and  $H_{90}$  (the 90-day harmonic representation of  $u'$ ) in Figure 3. The fraction of variance explained by  $H_{90}$  is quantified through its skill score ( $SS_{90}$ ), which we use as a common metric to compare internal-tide predictability at all stations. About one-third of the locations (color coded blue) have  $SS_{90} < 20\%$ , indicating that the internal tide is largely incoherent and unpredictable over 90-day periods. In contrast, the most-predictable location is the Timor Slope (color coded red), where 59% of the variance is predictable using 90-day harmonic fits. Five other locations (color coded orange) also exhibit some degree of predictability, with 38–51% of variance explained by  $H_{90}$ . At the remaining four stations (color coded green), only a modest 20–33% of internal tide variance is explained by 90-day harmonic fits. We conclude that only a relatively small fraction of the total baroclinic tidal-band variance is captured by long-time harmonic fits at most coastal locations. And at many locations, even the “predictable” component of the internal tide is only weakly correlated to the rms barotropic velocity (e.g., barotropic “spring tides”

do not necessarily correspond to large internal tides; compare red and black curves in Figure 1b). Next, we examine the geographic patterns of rms  $u_{bt}$ ,  $u'$ , and  $H_{90}$  (Figure 3).

On the western coast of the United States, the exposed shelf is relatively narrow, and the magnitude of the barotropic velocity is small ( $\leq 10 \text{ cm s}^{-1}$ ). A general increase toward larger  $u_{bt}$  moving northward is observed, perhaps consistent with the larger tidal range observed in the north (from  $\sim 0.5$  m off California to closer to  $\sim 1$  m off Washington (Egbert et al., 1994). The internal tide velocity tends to be of a similar magnitude as the barotropic velocity, and in general the variance recaptured by the 90-day harmonic fit is low, as quantified by  $SS_{90}$ . The only record that shows some predictive skill is the Washington Shelf ( $SS_{90} = 40\%$ ); however, it should be noted that this record is relatively short and is limited to two  $\sim 100$ -day spans that both occurred in summer.

On the broad eastern US coast, as well as on the Malin Shelf, barotropic velocities tend to be much greater ( $\geq 10 \text{ cm s}^{-1}$ ) than those observed along the western US coast. Those moorings located in sheltered and shallow ( $\sim 100$  m) water (i.e., off Key West, FL, and on the Maine Shelf) are exceptions to this trend. For the other stations, the variance in the internal tide is much smaller than that found in the barotropic velocity. Both the Malin Shelf and Maine Channel stations demonstrate a reasonable predictive skill, and a significant fraction of the variance in the baroclinic velocity is recovered by  $H_{90}$ . The same is true of the St. Augustine, FL, station, which is perhaps surprising because the mooring is located in very shallow water (37 m) and at a large distance from the shelf break.

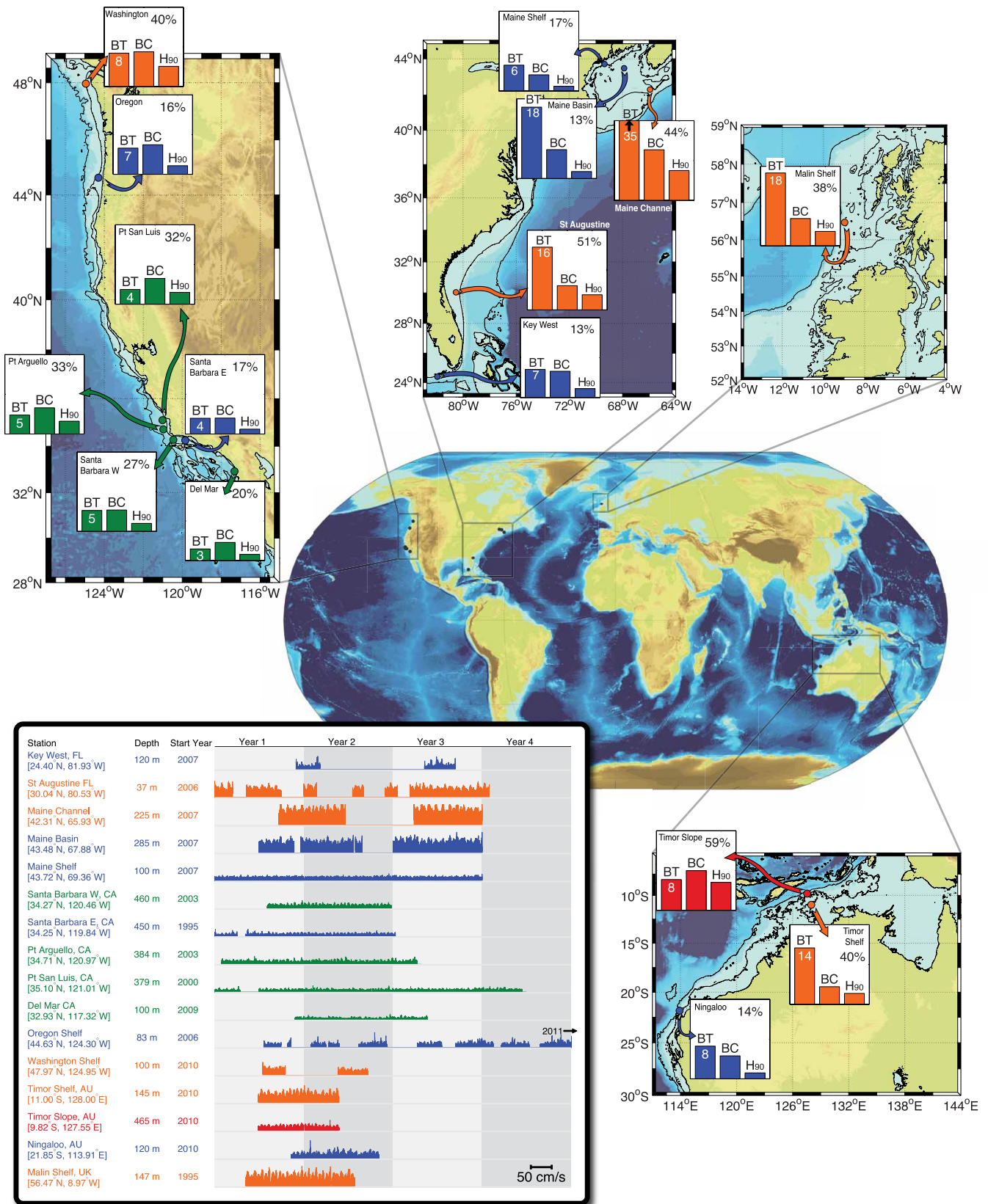


Figure 3. LOWER LEFT TABLE | Station names, locations, depth, and start year of data record. Subplots show  $\sqrt{u_{bt}^2 + v_{bt}^2}$  plotted over a four-year time span starting in January of Year 1; the gaps in plots indicate gaps in data records. With the exception of the Maine Channel, which is scaled by 75%, all plots are true to the velocity scale in the bottom right corner. Each mooring record is assigned a color based on predictability ( $SS_{90}$ ) with red/orange being more predictable than green/blue. MAP INSETS | Moving clockwise from the top left, insets show detailed bathymetry and mooring locations along the western US coast, eastern US coast, UK coast, and Australian coast. Bar plots for each mooring show the rms barotropic velocity, baroclinic velocity, and 90-day harmonic fit to the baroclinic velocity ( $H_{90}$ ). The magnitude for the barotropic component is given in  $\text{cm s}^{-1}$  (all plots use the same 0–20  $\text{cm s}^{-1}$  range). The skill of the 90-day harmonic fit ( $SS_{90}$ ) is indicated in the upper-right corner of each panel.

On the Australian North West Shelf, the surface-tide magnitude increases substantially from Ningaloo to the Timor Sea, and the shelf at Ningaloo is extremely narrow in contrast to the broad Timor Sea shelf. Internal-tide generation is likely remote from the Ningaloo site, and the water column there is well mixed in the austral winter. Both of these characteristics lead to low internal-tide predictability ( $SS_{90} = 14\%$ ). The depth of the Timor Sea shelf site is similar to that of the Ningaloo site and experiences similar seasonal variation in stratification, although the internal tide here is almost three times more predictable ( $SS_{90} = 40\%$ ). High predictability on the Timor Sea shelf is likely due to strong barotropic forcing and localized internal-tide generation over small-scale roughness. Even higher predictability on the Timor Sea slope is likely due to strong barotropic forcing, intense local internal-tide generation, and permanent stratification. Detailed results from the Timor Sea moorings are presented in Box 2.

## TIMESCALES OF PREDICTABILITY

To assess the duration over which the internal tide may be considered predictable (i.e., a substantial fraction of  $u'$  can be represented by  $H_T$ ), we computed  $SS_T$  for  $T$  ranging from three to 180 days, shown in Figure 4. At all locations, harmonic fits over short durations ( $\leq 7$  days) demonstrate significant skill ( $SS_T \geq 50\%$ ). However, as the duration of a harmonic fit increases,  $H_T$  captures less  $u'$  variance because it requires that the constituent signals retain their phase and amplitude over increasing time periods. This condition is expressed in terms of  $SS_T$ , which falls off at varying rates for the different locations. At many coastal locations (blue curves),  $SS_T \leq 30\%$  by  $T = 30$  days and less than 20% at  $T = 60$  days. For stations color coded green and orange, the decay with  $T$  is not as rapid; however, even for the most predictable of the shelf locations (e.g., St. Augustine, FL), only 52% of the variance can be explained with a 60-day harmonic fit.

We consider  $SS_{180}$  as a measure of the

fraction of velocity variance that remains coherent and predictable over  $O(1 \text{ year})$  durations. For more than three-quarters of the mooring sites, this predictable part represents less than one-third of the variance ( $SS_{180} < 30\%$ ) and can be as low as 8%. To quantify how quickly each time series becomes incoherent, we compute  $T_{50}$ , the timescale for harmonic analyses at which  $SS_T$  has been reduced halfway to its asymptotic value, which is approximated by  $SS_{180}$ . Figure 4 lists values of  $T_{50}$ .

Several conclusions can be drawn from  $T_{50}$ , the “timescale to incoherence.” First, we find that  $T_{50}$  retains similar ordering to  $SS_{180}$ . That is, locations where internal tides are more predictable generally maintain their predictability over longer timescales. Second,  $T_{50}$  is relatively short and similar at all locations. That is, the rate at which  $u'$  loses coherence (i.e.,  $SS_T$  moves toward its asymptotic, predictable value) is 1–2 weeks at all shelf sites, increasing to 19 days on the Timor slope. Thus, the incoherent part of the internal tide has a similar timescale of variability at all

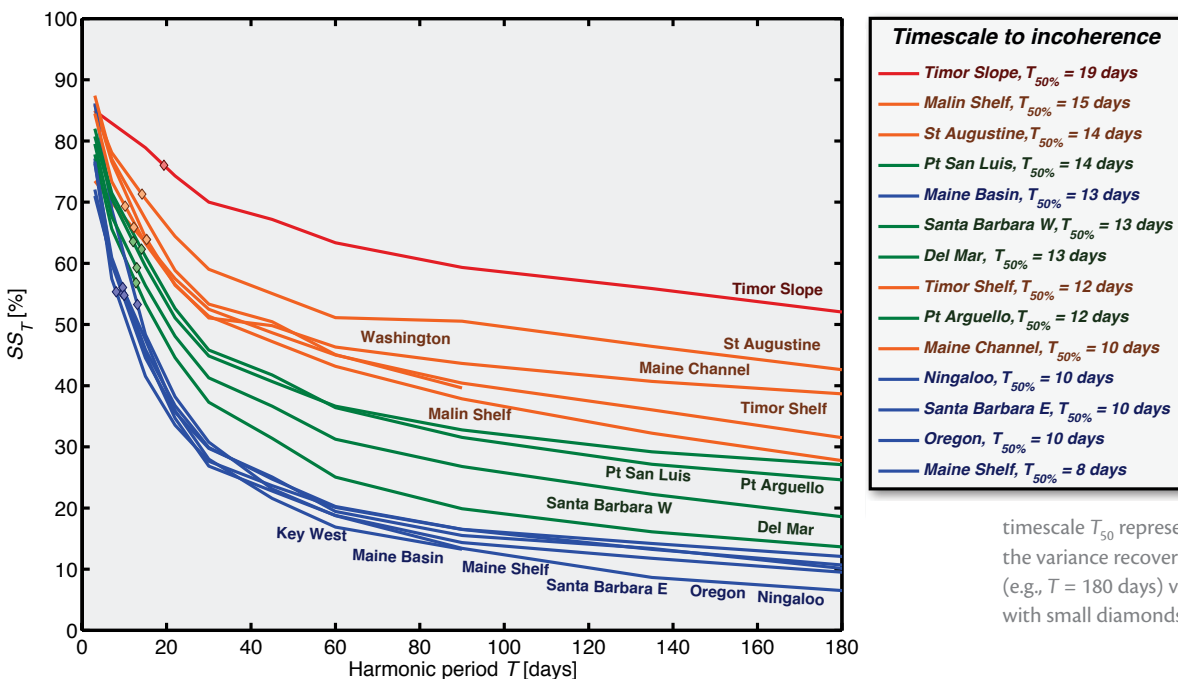


Figure 4. Fraction of the internal tide velocity variance recovered using harmonic fits of various durations ( $SS_T$ ) as a function of the duration of the fit ( $T$ ). In all cases, short-duration fits (e.g.,  $T = 7$  days) explain a significant fraction of the variance. For long time periods (e.g.,  $T \geq 180$  days),  $SS_T$  represents the fraction of variance of  $u'$  that is part of the stationary internal tide. The

timescale  $T_{50}$  represents the duration for which the variance recovered is halfway to its stationary (e.g.,  $T = 180$  days) value, indicated in the figure with small diamonds.

shelf locations—whether they are largely predictable (like St. Augustine or Malin) or not (like Ningaloo or Oregon). This consistency suggests that the processes responsible for coherence loss primarily operate on relatively short timescales (days to a few weeks), and similarly at all locations. A likely mechanism for introducing such variability is the mesoscale, which often exhibits pattern changes on 5–20 day timescales, and could alter how internal tides are generated locally, how they propagate, and how waves from multiple sources interfere with each other. At the same time, the mesoscale is also responsible for Doppler shifting internal tides propagating through the open ocean (Rainville and Pinkel, 2006; Arbic et al., 2012, in this issue), which scrambles wave arrival times and creates groupiness of the shoaling “internal swell” on 5–20 day timescales (e.g., Nash et al., 2004).

It is worth noting that temporal incoherence does not necessarily imply spatial incoherence on a continental shelf. This is because a 50–300 km wide shelf is transited by an internal tide in 1–6 days, a timescale over which internal tides are generally coherent. As a result, internal tides have been observed with spatial coherence over scales of several hundred kilometers (Pingree and New, 1995), implying a degree of coherence over days to weeks, but not months. This spatial coherence is consistent with our estimates of  $T_{50} \sim 10$  days. Synoptic studies of internal tides and nonlinear internal waves (e.g., Shroyer et al., 2010b; Inall et al., 2011) show that wave crests can be traced great distances in the direction of propagation ( $\sim 100$  km). These studies also show the observed spatial decay rate to be consistent with observed energy dissipation at the turbulent microscale ( $\sim$  centimeter scale). Correlation scale

lengths in the along-crest direction, including wavefront curvature effects, are less well documented, but are known from satellite images to be geographically variable. On many continental shelves, we thus expect the spatial patterns of the internal tide to be linked more strongly to details of the bathymetry and local physical dynamics, as opposed to loss of spatial coherence associated with the temporal modulation presented here.

### IMPLICATIONS FOR COASTAL CIRCULATION/CONSEQUENCES OF INTERMITTENCY

Here, we have examined time series of internal-tide velocity obtained at a diverse set of locations in coastal seas. All the time series exhibited phase and amplitude variability in the internal tide on a range of temporal scales. We attribute this incoherency to changes in stratification, mesoscale currents, and the shoaling of “internal swell,” which act together to infuse variability into the internal tide. The 16 time series examined here contain each of these processes in different proportions, and our analysis of the internal-tide incoherency (or predictability) at different locations does not allow for consideration of these factors individually. However, at least one generality emerges: more than 50% of internal tide energy in the coastal ocean appears to be universally unpredictable by harmonic fits over periods longer than 20 days. This finding—which spans analyses across coastal seas with different geometry, stratification, barotropic forcing, and mesoscale variability—suggests that multiple mechanisms (or combinations of mechanisms) cause the internal tide to lose coherence. Therefore, increasing the accuracy of internal-tide prediction undoubtedly requires a multifaceted strategy to better represent a

number of dynamical processes.


In this article, we have assessed internal-tide predictability solely on the basis of harmonic analysis. Shelf sea models are more sophisticated than this because they can simulate and resolve a wide range of sub- and super-tidal processes that may modulate internal-tide generation and propagation (Carter et al., 2012, in this issue). Therefore, some of the energy that is unpredictable from harmonic analysis may be simulated in a regional model. However, even models that accurately represent the mesoscale and tidal forcing show poor skill in deterministically predicting the timing of internal tide pulses (e.g., Osborne et al., 2011), likely because coastal internal tide predictions are so sensitive to subtle details of stratification and fine-scale bathymetry. We note, however, that these models can represent the statistics of the internal tide reasonably well. From a regional modeling perspective, distinguishing between local and remote sources of internal tidal energy may be a critical factor for these discrepancies. The recognition that amplitudes and phases of internal tides at many sites may depend on shoaling “internal swell” means that modeling of the low-mode internal tide on a global scale (e.g., Arbic et al., 2012, in this issue) may be a prerequisite for detailed prediction of coastal internal tides. This prediction would require a high degree of information regarding the oceanic mesoscale state, possibly obtainable by data assimilative models that incorporate information from satellites, profiling floats, and other observational platforms.

Assessing the predictability of internal tides is important both for marine operational reasons and for broader research investigations. An intermittent and unpredictable internal tide can

decrease the accuracy of sonar, endanger offshore structures and operations, and lead to uncertainty in previous estimates of cross-shelf transport and diapycnal mixing. Research over the last few decades has emphasized the global significance of the internal tide, which together with near-inertial waves, is one of the most energetic components of the internal wave spectrum. Internal tides can therefore cascade significant energy to shorter and higher-frequency internal waves that eventually drive turbulent mixing (Smyth and Moum, 2012, and Venayagamoorthy and Fringer, 2012, both in this issue). Perhaps as much as 60% of internal-tide energy is dissipated on the outer shelf (Holloway et al., 2001; Inall et al., 2011), where it contributes to diapycnal mixing and cross-margin exchanges, thereby impacting the nutrient and heat budgets on the shelf.

In the coastal ocean, vertical mixing by internal tides contributes to both the buoyancy and nutrient fluxes (Pingree and Mardell, 1981; Sharples et al., 2009). Furthermore, internal waves are not only thought to redistribute energy across the shelf (thus influencing the spatial structure of turbulent mixing) but they also can transport mass. In particular, the cross-shelf transport of multiple species of invertebrate larvae and small fish has been linked to internal wave activity (e.g., Kingsford and Choat, 1986; Pineda, 1999; Shanks, 2006). The internal tide may even affect predator-prey relations high in the food chain, for example, by large-amplitude internal waves bringing fish close to the surface where they may become prey for seabirds (Jonathan Sharples, Natural Environment Research Council (UK), author Inall, and colleagues, *pers. comm.*, 2012).

## ACKNOWLEDGEMENTS

We thank Uwe Send and Matthew Alford for graciously contributing data from their Del Mar and Washington moorings for these analyses. Other data were collected using the support of the US National Science Foundation (NSF), US National Oceanic and Atmospheric Administration, and Australian Institute of Marine Science (AIMS). This work was supported through grants from the US Office of Naval Research and NSF (Nash, Shroyer, Musgrave, Levine, and Duda), by NERC (grant NE/IO30224/1 FASTNet; Inall), and by AIMS/CSIRO (Kelly and Jones). 

## REFERENCES

Alford, M.H. 2001. Internal swell generation: The spatial distribution of energy flux from the wind to mixed layer near-inertial motions. *Journal of Physical Oceanography* 31:2,359–2,368, [http://dx.doi.org/10.1175/1520-0485\(2001\)031<2359:ISGTSD>2.0.CO;2](http://dx.doi.org/10.1175/1520-0485(2001)031<2359:ISGTSD>2.0.CO;2).

Alford, M.H. 2003. Redistribution of energy available for ocean mixing by long-range propagation of internal waves. *Nature* 423:159–162, <http://dx.doi.org/10.1038/nature01628>.

Alford, M.H., and Z. Zhao. 2007. Global patterns of low-mode internal-wave propagation. Part I: Energy and energy flux. *Journal of Physical Oceanography* 37:1,829–1,848, <http://dx.doi.org/10.1175/JPO3085.1>.

Arbic, B.K., J.G. Richman, J.F. Shriver, P.G. Timko, E.J. Metzger, and A.J. Wallcraft. 2012. Global modeling of internal tides within an eddying ocean general circulation model. *Oceanography* 25(2):20–29, <http://dx.doi.org/10.5670/oceanog.2012.38>.

Baines, P.G. 1982. On internal tide generation models. *Deep-Sea Research Part A* 29:307–338, [http://dx.doi.org/10.1016/0198-0149\(82\)90098-X](http://dx.doi.org/10.1016/0198-0149(82)90098-X).

Boehm, A.B., B.F. Sanders, and C.D. Winant. 2002. Cross-shelf transport at Huntington Beach. Implications for the fate of sewage discharged through an offshore ocean outfall. *Environmental Science & Technology* 36:1,899–1,906, <http://dx.doi.org/10.1021/es0111986>.

Briscoe, M.G. 1984. Oceanography: Tides, solitons and nutrients. *Nature* 312:15, <http://dx.doi.org/10.1038/312015a0>.

Carter, G.S., O.B. Fringer, and E.D. Zaron. 2012. Regional models of internal tides. *Oceanography* 25(2):56–65, <http://dx.doi.org/10.5670/oceanog.2012.42>.

Carter, G.S., M.A. Merrifield, J.M. Becker, K. Katsumata, M.C. Gregg, D.S. Luther, M.D. Levine, T.J. Boyd, and Y.L. Firing. 2008.

Energetics of M2 barotropic-to-baroclinic tidal conversion at the Hawaiian Islands. *Journal of Physical Oceanography* 38:2,205–2,223, <http://dx.doi.org/10.1175/2008JPO3860.1>.

Colosi, J.A., and W. Munk. 2006. Tales of the venerable Honolulu tide gauge. *Journal of Physical Oceanography* 36:967–996, <http://dx.doi.org/10.1175/JPO2876.1>.

Cottier, F., M. Inall, and G. Griffiths. 2004. Seasonal variations in internal wave energy in a Scottish sea loch. *Ocean Dynamics* 54:340–347, <http://dx.doi.org/10.1007/s10236-003-0064-5>.

Dushaw, B.D., P.F. Worcester, and M.A. Dzieciuch. 2011. On the predictability of mode-1 internal tides. *Deep Sea Research Part I* 58:677–698, <http://dx.doi.org/10.1016/j.dsr.2011.04.002>.

Egbert, G.D., A.F. Bennett, and M.G.G. Foreman. 1994. TOPEX/POSEIDON tides estimated using a global inverse model. *Journal of Geophysical Research* 99:24,821–24,852, <http://dx.doi.org/10.1029/94JC01894>.

Garrett, C. 1972. Tidal resonance in the Bay of Fundy and Gulf of Maine. *Nature* 238:441–443, <http://dx.doi.org/10.1038/238441a0>.

Gerkema, T., F.P.A. Lam, and L.R.M. Maas. 2004. Internal tides in the Bay of Biscay: Conversion rates and seasonal effects. *Deep Sea Research Part II* 51:2,995–3,008, <http://dx.doi.org/10.1016/j.dsr2.2004.09.012>.

Green, J.A.M., J.H. Simpson, S. Legg, and M.R. Palmer. 2008. Internal waves, baroclinic fluxes and mixing at the European shelf edge. *Continental Shelf Research* 28:937–950, <http://dx.doi.org/10.1016/j.csr.2008.01.014>.

Holloway, P.E. 1988. Climatology of internal tides at a shelf-break location on the Australian North West Shelf. *Marine and Freshwater Research* 39:1–18, <http://dx.doi.org/10.1071/MF9880001>.

Holloway, P.E., P.G. Chatwin, and P. Craig. 2001. Internal tide observations from the Australian north west shelf in summer 1995. *Journal of Physical Oceanography* 31:1,182–1,199, [http://dx.doi.org/10.1175/1520-0485\(2001\)031<1182:ITOFTA>2.0.CO;2](http://dx.doi.org/10.1175/1520-0485(2001)031<1182:ITOFTA>2.0.CO;2).

Inall, M.E., T.P. Rippeth, and T.J. Sherwin. 2000. Impact of nonlinear waves on the dissipation of internal tidal energy at a shelf break. *Journal of Geophysical Research* 105:8,687–8,705, <http://dx.doi.org/10.1029/1999JC900299>.

Inall, M., D. Aleynik, T. Boyd, M. Palmer, and J. Sharples. 2011. Internal tide coherence and decay over a wide shelf sea. *Geophysical Research Letters* 38, L23607, <http://dx.doi.org/10.1029/2011GL049943>.

Kelly, S.M., and J.D. Nash. 2010. Internal-tide generation and destruction by shoaling internal tides. *Geophysical Research Letters* 37, L23611, <http://dx.doi.org/10.1029/2010GL045598>.

Kingsford, M.J., and J.H. Choat. 1986. Influence of surface slicks on the distribution and onshore movements of small fish. *Marine Biology* 91:161–171, <http://dx.doi.org/10.1007/BF00569432>.

Lee, C.M., E. Kunze, T.B. Sanford, J.D. Nash, M.A. Merrifield, and P.E. Holloway. 2006. Internal tides and turbulence along the 3000-m



- isobath of the Hawaiian Ridge. *Journal of Physical Oceanography* 36:1,165–1,183, <http://dx.doi.org/10.1175/JPO2886.1>.
- Lerczak, J.A., C.D. Winant, and M.C. Hendershott. 2003. Observations of the semidiurnal internal tide on the southern California slope and shelf. *Journal of Geophysical Research* 108, 3068, <http://dx.doi.org/10.1029/2001JC001128>.
- Li, Q., and D.M. Farmer. 2011. The generation and evolution of nonlinear internal waves in the deep basin of the South China Sea. *Journal of Physical Oceanography* 41:1,345–1,363, <http://dx.doi.org/10.1175/2011JPO4587.1>.
- Lim, K., G.N. Ivey, and R.L. Nokes. 2008. The generation of internal waves by tidal flow over continental shelf/slope topography. *Environmental Fluid Mechanics* 8:511–526, <http://dx.doi.org/10.1007/s10652-008-9085-4>.
- MacKinnon, J.A., and M.C. Gregg. 2003. Shear and baroclinic energy flux on the summer New England shelf. *Journal of Physical Oceanography* 33:1,462–1,475, [http://dx.doi.org/10.1175/1520-0485\(2003\)033<1462:SABEFO>2.0.CO;2](http://dx.doi.org/10.1175/1520-0485(2003)033<1462:SABEFO>2.0.CO;2).
- Martini, K.I., M.H. Alford, E. Kunze, S.M. Kelly, and J.D. Nash. 2011. Observations of internal tides on the Oregon continental slope. *Journal of Physical Oceanography* 41:1,772–1,794, <http://dx.doi.org/10.1175/2011JPO4581.1>.
- Moum, J.N., J.D. Nash, and J.M. Klymak. 2008. Small-scale processes in the coastal ocean. *Oceanography* 21(4):22–33, <http://dx.doi.org/10.5670/oceanog.2008.02>.
- Murphy, A.H. 1988. Skill scores based on the mean square error and their relationships to the correlation coefficient. *Monthly Weather Review* 116:2,417–2,424, [http://dx.doi.org/10.1175/1520-0493\(1988\)116<2417:SSBOTM>2.0.CO;2](http://dx.doi.org/10.1175/1520-0493(1988)116<2417:SSBOTM>2.0.CO;2).
- Nash, J. D., S.M. Kelly, E.L. Shroyer, J.N. Moum, and T.F. Duda. In press. The unpredictable nature of internal tides on the continental shelf. *Journal of Physical Oceanography*.
- Nash, J.D., E. Kunze, J.M. Toole, and R.W. Schmitt. 2004. Internal tide reflection and turbulent mixing on the continental slope. *Journal of Physical Oceanography* 34:1,117–1,134, [http://dx.doi.org/10.1175/1520-0485\(2004\)034<1117:ITRATM>2.0.CO;2](http://dx.doi.org/10.1175/1520-0485(2004)034<1117:ITRATM>2.0.CO;2).
- Noble, M., B. Jones, P. Hamilton, J. Xu, G. Robertson, L. Rosenfeld, and J. Largier. 2009. Cross-shelf transport into nearshore waters due to shoaling internal tides in San Pedro Bay, CA. *Continental Shelf Research* 29:1,768–1,785, <http://dx.doi.org/10.1016/j.csr.2009.04.008>.
- Osborne, A.R., T.L. Burch, and R.I. Scarlet. 1978. The influence of internal waves on deep-water drilling. *Journal of Petroleum Technology* 30:1,497–1,504, <http://dx.doi.org/10.2118/6913-PA>.
- Osborne, J.J., A.L. Kurapov, G.D. Egbert, and P.M. Kosro. 2011. Spatial and temporal variability of the M2 internal tide generation and propagation on the Oregon shelf. *Journal of Physical Oceanography* 41:2,037–2,062, <http://dx.doi.org/10.1175/JPO-D-11-02.1>.
- Pineda, J. 1999. Circulation and larval distribution in internal tidal bore warm fronts. *Limnology and Oceanography* 44:1,400–1,414.
- Pingree, R.D., G.T. Mardell, and A.L. New. 1986. Propagation of internal tides from the upper slopes of the Bay of Biscay. *Nature* 321:154–158, <http://dx.doi.org/10.1038/321154a0>.
- Pingree, R.D., and G.T. Mardell. 1981. Slope turbulence, internal waves and phytoplankton growth at the Celtic Sea shelf-break. *Royal Society of London Philosophical Transactions Series A* 302:663–678, <http://dx.doi.org/10.1098/rsta.1981.0191>.
- Pingree, R.D., and A.L. New. 1991. Abyssal penetration and bottom reflection of internal tide energy into the Bay of Biscay. *Journal of Physical Oceanography* 21:28–39, [http://dx.doi.org/10.1175/1520-0485\(1991\)021<0028:APABRO>2.0.CO;2](http://dx.doi.org/10.1175/1520-0485(1991)021<0028:APABRO>2.0.CO;2).
- Pingree, R., and A. New. 1995. Structure, seasonal development and sunglint spatial coherence of the internal tide on the Celtic and Armorican shelves and in the Bay of Biscay. *Deep Sea Research Part I* 42:245–284, [http://dx.doi.org/10.1016/0967-0637\(94\)00041-P](http://dx.doi.org/10.1016/0967-0637(94)00041-P).
- Rainville, L., T.M.S. Johnston, G.S. Carter, M.A. Merrifield, R. Pinkel, P.F. Worcester, and B.D. Dushaw. 2010. Interference pattern and propagation of the M2 internal tide south of the Hawaiian Ridge. *Journal of Physical Oceanography* 40:311–325, <http://dx.doi.org/10.1175/2009JPO4256.1>.
- Rainville, L., and R. Pinkel. 2006. Propagation of low-mode internal waves through the ocean. *Journal of Physical Oceanography* 36:1,220–1,236, <http://dx.doi.org/10.1175/JPO2889.1>.
- Ramp, S.R., Y.J. Yang, and F.L. Bahr. 2010. Characterizing the nonlinear internal wave climate in the northeastern South China Sea. *Nonlinear Processes in Geophysics* 17:481–498, <http://dx.doi.org/10.5194/npg-17-481-2010>.
- Rayson, M.D., G.N. Ivey, N.L. Jones, M.J. Meuleners, and G.W. Wake. 2011. Internal tide dynamics in a topographically complex region: Browse Basin, Australian North West Shelf. *Journal of Geophysical Research* 116, C01016, <http://dx.doi.org/10.1029/2009JC005881>.
- Savidge, D.K., C.R. Edwards, and M. Santana. 2007. Baroclinic effects and tides on the Cape Hatteras continental shelf. *Journal of Geophysical Research* 112, C09016, <http://dx.doi.org/10.1029/2006JC003832>.
- Scotti, A., R.C. Beardsley, B. Butman, and J. Pineda. 2008. Shoaling of nonlinear internal waves in Massachusetts Bay. *Journal of Geophysical Research* 113, C08031, <http://dx.doi.org/10.1029/2008JC004726>.
- Shanks, A.L. 2006. Mechanisms of cross-shelf transport of crab megalopae inferred from a time series of daily abundance. *Marine Biology* 148:1,383–1,398, <http://dx.doi.org/10.1007/s00227-005-0162-7>.
- Sharples, J., J.F. Tweddle, J.A. Mattias Green, M.R. Palmer, Y.-N. Kim, A.E. Hickman, P.M. Holligan, C.M. Moore, T.P. Rippeth, J.H. Simpson, and V. Krivtsov. 2007. Spring-neap modulation of internal tide mixing and vertical nitrate fluxes at a shelf edge in summer. *Limnology and Oceanography* 52(5):1,735–1,747.
- Sharples, J., C.M. Moore, A.E. Hickman, P.M. Holligan, J.F. Tweddle, M.R. Palmer, and J.H. Simpson. 2009. Internal tidal mixing as a control on continental margin ecosystems. *Geophysical Research Letters* 36, L23603, <http://dx.doi.org/10.1029/2009GL040683>.
- Shearman, R.K., and K.H. Brink. 2010. Evaporative dense water formation and cross-shelf exchange over the northwest Australian inner shelf. *Journal of Geophysical Research* 115, C06027, <http://dx.doi.org/10.1029/2009JC005931>.
- Sherwin, T.J. 1988. Analysis of an internal tide observed on the Malin Shelf, north of Ireland. *Journal of Physical Oceanography* 18:1,035–1,050, [http://dx.doi.org/10.1175/1520-0485\(1988\)018<1035:AOAITO>2.0.CO;2](http://dx.doi.org/10.1175/1520-0485(1988)018<1035:AOAITO>2.0.CO;2).
- Sherwin, T.J., V.I. Vlasenko, N. Stashchuk, D.R. Jeans, and B. Jones. 2002. Along-slope generation as an explanation for some unusually large internal tides. *Deep Sea Research Part I* 49:1,787–1,799, [http://dx.doi.org/10.1016/S0967-0637\(02\)00096-1](http://dx.doi.org/10.1016/S0967-0637(02)00096-1).
- Shroyer, E.L., J.N. Moum, and J.D. Nash. 2010a. Vertical heat flux and lateral mass transport in nonlinear internal waves. *Geophysical Research Letters* 37, L08601, <http://dx.doi.org/10.1029/2010GL042715>.
- Shroyer, E.L., J.N. Moum, and J.D. Nash. 2010b. Energy transformations and dissipation of nonlinear internal waves over New Jersey's continental shelf. *Nonlinear Processes in Geophysics* 17:345–360, <http://dx.doi.org/10.5194/npg-17-345-2010>.
- Smyth, W.D., and J.N. Moum. 2012. Ocean mixing by Kelvin-Helmholtz instability. *Oceanography* 25(2):140–149, <http://dx.doi.org/10.5670/oceanog.2012.49>.
- Souza, A.J., J.H. Simpson, M. Harikrishnan, and J.J. Malarkey. 2001. Flow structure and seasonality in the Hebridean slope current. *Oceanologica Acta* 24:63–76, [http://dx.doi.org/10.1016/S0399-1784\(00\)01103-8](http://dx.doi.org/10.1016/S0399-1784(00)01103-8).
- Thomas, H., Y. Bozec, and H.J.W. de Baar. 2004. Enhanced open ocean storage of CO<sub>2</sub> from shelf sea pumping. *Science* 304:1,005–1,008, <http://dx.doi.org/10.1126/science.1095491>.
- Van Gastel, P., G.N. Ivey, M.J. Meuleners, J.P. Antenucci, and O. Fringer. 2009. The variability of the large-amplitude internal wave field on the Australian North West Shelf. *Continental Shelf Research* 29:1,373–1,383, <http://dx.doi.org/10.1016/j.csr.2009.02.006>.
- Venayagamoorthy, S.K., and O.B. Fringer. 2012. Examining breaking internal waves on a shelf slope using numerical simulations. *Oceanography* 25(2):132–139, <http://dx.doi.org/10.5670/oceanog.2012.48>.
- Wunsch, C. 1975. Internal tides in the ocean. *Reviews of Geophysics* 13:167–182, <http://dx.doi.org/10.1029/RG013i001p0167>.
- Zilberman, N.V., M.A. Merrifield, G.S. Carter, D.S. Luther, M.D. Levine, and T.J. Boyd. 2011. Incoherent nature of M<sub>2</sub> internal tides at the Hawaiian Ridge. *Journal of Physical Oceanography* 41:2,021–2,036, <http://dx.doi.org/10.1175/JPO-D-10-05009.1>.